

First-principles study of electronic structure of $\text{Bi}_2\text{Sr}_2\text{Ca}_2\text{Cu}_3\text{O}_{10}$

J. A. Camargo-Martínez, Diego Espitia and R. Baquero

Departamento de Física, Centro de Investigación y de Estudios Avanzados del Instituto Politécnico Nacional, Av. IPN 2508, 07360 México

Received 25 July 2013; accepted 3 October 2013

We present for the first time the electronic structure calculation of $\text{Bi}_2\text{Sr}_2\text{Ca}_2\text{Cu}_3\text{O}_{10}$ compound in the tetragonal structure (space group $I4/mmm$). We used the Local Density Approximation (LDA) as in the Wien2k code. We analyze in detail the band structure, density of states, and Fermi surface (FS) for this compound. The FS calculated shows the feature known as the Bi-O pocket problem which we associate with the interaction of the Cu2-O2 and Bi-O4 planes through O3 atoms. However, our FS in the nodal direction is in very good agreement with the FS measured using angle-resolved photo-emission spectroscopy (ARPES). This calculation is useful, since $\text{Bi}_2\text{Sr}_2\text{Ca}_2\text{Cu}_3\text{O}_{10}$ compound show a transition to the superconducting state at ~ 110 K and to date there are no reports in the literature of its electronic structure known to us.

Keywords: Bi-2223; electronic structure; band structure; Fermi surface.

PACS: 74.72.Hs; 71.20.-b; 71.18.+y; 73.20.At

1. Introduction

Bismuth cuprates are high-temperature superconductors (HTSC) (except Bi-2201 with $T_c \sim 2$ K) with the general formula $\text{Bi}_2\text{Sr}_2\text{Ca}_{n-1}\text{Cu}_n\text{O}_y$. They are normally referred to by the number of CuO_2 planes per unit cell, as Bi-2201, Bi-2212, Bi-2223 and Bi-2234 ($n = 1, 2, 3$ and 4 respectively). Resistivity, susceptibility and magnetization experiments performed on Bi-2212 and Bi-2223 show a transition to the superconducting state at ~ 85 K [1,2] and ~ 110 K [3,4] respectively.

The electronic properties of Bi-2212 have been extensively studied both theoretically and experimentally [5-10]. To our best knowledge a theoretical study of the Bi-2223 compound has not been yet reported in the literature in spite of the fact that this compound is one of the most suitable HTSC materials for applications [11-13]. Neutron and X-ray diffraction experiments suggest that Bi-2223 presents several orthogonal structures with spacial groups $Amaa$, $A2aa$ and $Fmmm$ [14-16] and a tetragonal structure with spatial group $I4/mmm$ [17,18]. This structure seems to be more stable when doped with Pb [16-20]. Recently experimental studies of the electronic structure of Bi-2223 by angle-resolved photo-emission spectroscopy (ARPES) have been reported [21-24]. In particular, Ideta *et al.* [23] report a band splitting at the Fermi surface in the nodal direction associated with the outer and inner CuO_2 planes (OP and IP).

In this work we present a detailed study of the electronic band structure, the density of states and the Fermi surface (FS) for Bi-2223. Also we present the comparison between our FS calculation and the experimental results reported by Ideta *et al.* [23].

2. Method of Calculation

The electronic properties for $\text{Bi}_2\text{Sr}_2\text{Ca}_2\text{Cu}_3\text{O}_{10}$ were determined with the full-potential linearized augmented plane

wave method plus local orbital (FLAPW+lo) [25] within the local density approximation (LDA) using the wien2k code [26]. The core states are treated fully relativistically, while for the valence states the scalar relativistic approximation is used. We used a plane-wave cutoff of $R_{\text{mt}}K_{\text{max}}=8.0$ and for the wave function expansion inside the atomic spheres, a maximum value of the angular momentum of $l_{\text{max}}=12$ with $G_{\text{max}}=25$. We choose a $17 \times 17 \times 17$ k-space grid which contains 405 points within the irreducible wedge of the Brillouin zone. The muffin-tin sphere radii R_{mt} (in atomic units) are chosen as 2.3 for Bi, 2.0 for Sr, 1.9 for both Ca and Cu, and 1.5 for O.

3. The Bi-2223 crystal structure

In this work, we study the Bi-2223 compound with body center tetragonal structure (bct) and space group $I4/mmm$ (D_{4h}^{17}). The structure consists of three Cu-O planes, one Cu1-O1 plane between two Cu2-O2 planes, with Ca atoms between them. Each Cu2-O2 plane is followed by a Sr-O3 and Bi-O4 planes in that order (see Fig. 1).

Starting from the experimental parameters taken from Ref. 17, we optimized the c/a ratio by minimization of the total energy and relaxed the internal coordinates of the structure by minimization of forces. In Table I we compare these results with the experimental values reported. The optimized c/a ratio is 1.56% smaller than the experimental one. In the relaxed structure the Cu1-O1 and Cu2-O2 planes approach each other by ~ 0.5 Å while the distance between the Cu2-O2 and Bi-O4 planes increases by ~ 0.3 Å as compared to the experimental values. The Sr atoms keep their distance to the Cu2-O2 planes while the O3 atoms move away from the Cu2 ones towards the bismuth atoms.

The main difference between the crystal structure of Bi-2212 [6] and Bi-2223 is the presence of the new CuO_2 plane

TABLE I. Optimized and relaxed structural parameters of the tetragonal $\text{Bi}_2\text{Sr}_2\text{Ca}_2\text{Cu}_3\text{O}_{10}$. The experimental values were taken from reference 17.

Space group $I4/mmm, z=2$		
	Expt.	This work
a	3.823Å	3.843Å
c	37.074Å	36.686Å
c/a	9.70	9.55
atom	z	z
Bi	0.2109	0.2072
Sr	0.3557	0.3682
Ca	0.4553	0.4573
Cu1	0.0000	0.0000
Cu2	0.0976	0.0839
O1	0.0000	0.0000
O2	0.0964	0.0847
O3	0.1454	0.1519
O4	0.2890	0.2936

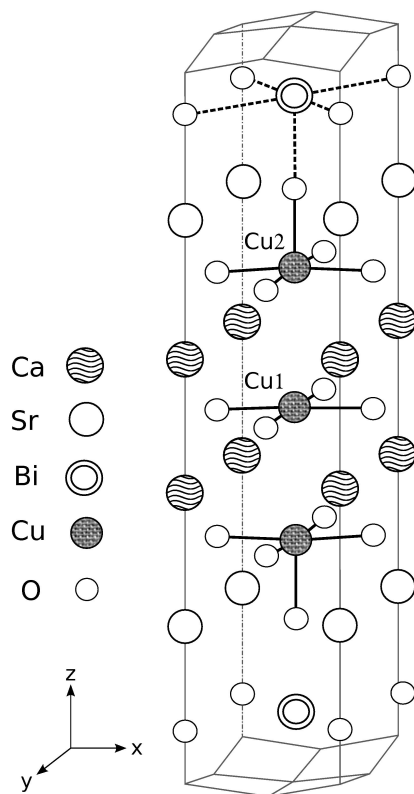


FIGURE 1. Primitive cell for body-centered tetragonal $\text{Bi}_2\text{Sr}_2\text{Ca}_2\text{Cu}_3\text{O}_{10}$. O1, O2, O3 and O4 denote oxygens in the Cu1, Cu2, Sr and Bi planes, respectively.

in the last one labeled in this work as Cu1-O1. The lattice parameter a is identical in both structures but the c one differs by ~ 7 Å. The presence of the new plane changes the inter-

layer distance between neighboring copper-oxygen planes. In Bi-2223, the inter-layer CuO_2 distance is ~ 0.38 Å larger than in Bi-2212. We will show the contribution in the electronic structure due Cu1-O1 plane.

4. Results and discussion

4.1. The density of states

Figure 2 shows both the total Density of States (DOS) and the atom-projected densities of states (pDOS). We found that the Fermi level, E_F , falls in a region of low DOS. This behavior is similar to others Cu-O-based superconductors [27-30]. As might be expected, the Bi-2223 compound maintains the same behavior as the DOS in the Bi-2212 compound [6-9], the only difference is the contribution of the new Cu1-O1 plane. The total density of states at E_F , $N(E_F)$, for Bi-2223 is 3.55 states/(eV cell) which is larger than the one reported

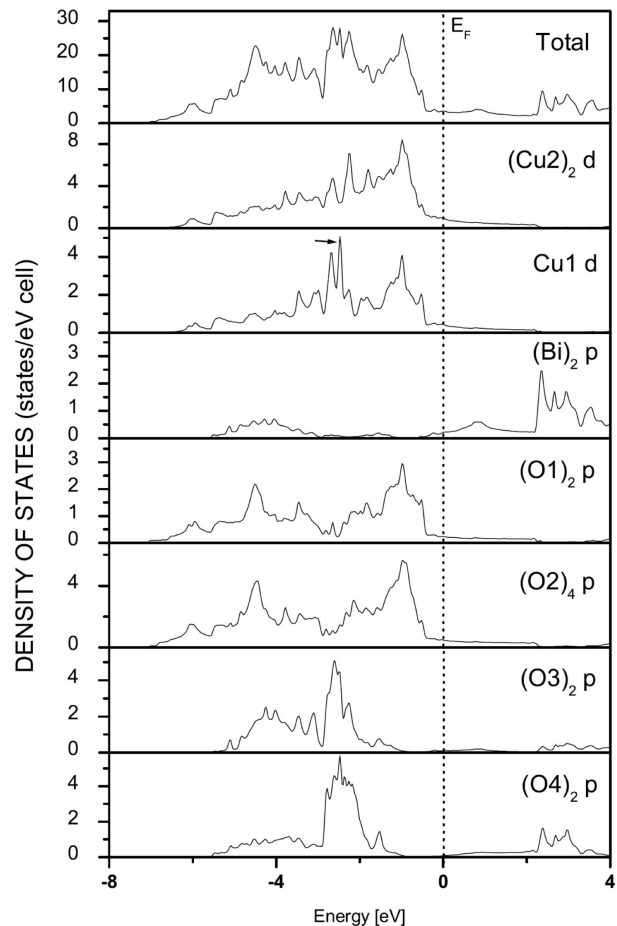


FIGURE 2. Total and atom-projected density of states for $\text{Bi}_2\text{Sr}_2\text{Ca}_2\text{Cu}_3\text{O}_{10}$. Note the change of scale for each atom contribution. The arrow in the pDOS of Cu1 d indicates the peak at 2.49 eV below E_F .

TABLE II. Atomic contributions to the density of states at the Fermi level, $N(E_F)$, for both Bi-2212 and Bi-2223. The values are given in units of states/eV-atom. The total $N(E_F)$ is in units of states/(eV cell). The data for Bi-2212 were taken from Ref. 9.

Compound	Atomic state							Total $N(E_F)$
	Cu2 d	Cu1 d	Bi p	O1 p	O2 p	O3 p	O4 p	
Bi-2212	-	0.33	0.17	0.16	0.07	0.07	-	2.88
Bi-2223	0.47	0.44	0.10	0.12	0.12	0.06	0.04	3.55

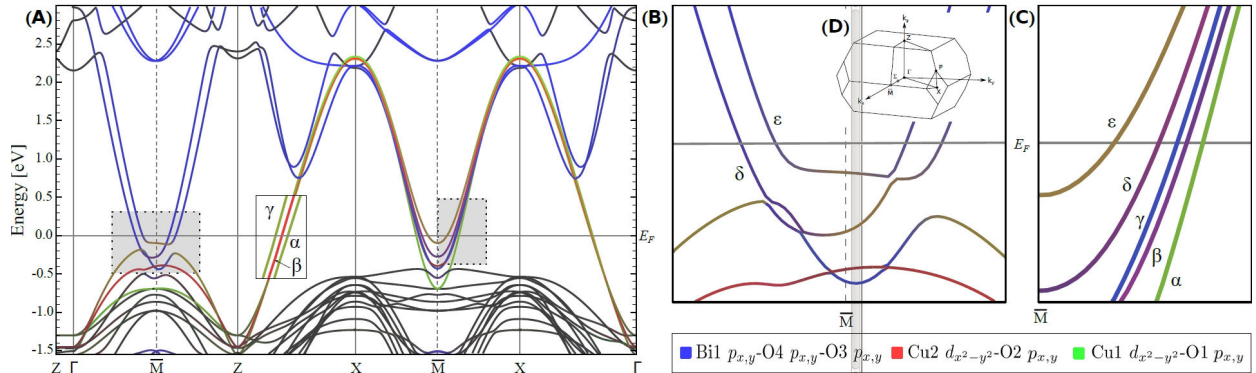


FIGURE 3. (Color online) The band structure of the $\text{Bi}_2\text{Sr}_2\text{Ca}_2\text{Cu}_3\text{O}_{10}$ compound. Note that the behavior of the bands are similar along the X-Z and the X- Γ directions. The shaded areas in the figure (A) are amplified in Figures (B) and (C) respectively. In (D) we show the first Brillouin zone for a body-centered tetragonal structure for completeness.

for Bi-2212 (2.1-3.3 states/(eV cell)) [6,8] (see Table II). In the Bi-2223 compound a large contribution comes from the Cu2-O2, Cu1-O1 and Bi-O4 planes. The Bi-O plane contributes with small electron pockets at the Fermi surface providing conduction electrons. These pockets, nevertheless, do not appear in the experimental results [31]. It is important to note that the new Cu1-O1 plane contributes significantly to $N(E_F)$. On the other hand, comparing the atomic contributions to $N(E_F)$ in both compound (see Table II), we observe a larger contribution of Cu2-O2 planes in Bi-2223 and a similar one from the Bi-O4 planes. The composition at E_F of the Bi-2223 DOS is mainly as follows, Cu2 $d_{x^2-y^2}$, O2 $p_{x,y}$, Cu1 $d_{x^2-y^2}$, O1 $p_{x,y}$, Bi $p_{x,y}$, O4 $p_{x,y}$ and O3 $p_{x,y,z}$ states.

In Fig. 2 we observe that the contribution of the d-states to the pDOS from the Cu1 and Cu2 atoms is very similar. The only difference is the peak at 2.49 eV below E_F which corresponds to the contribution of the Cu1 $d_{xz,yz}$ states. The occupied bandwidth of the Cu-O planes is ~ 7 eV. Also observe the wide bandwidth of ~ 9 eV which is typical of the $dp\sigma$ (bonding and anti-bonding) bands from the two-dimensional CuO_2 layers [29]. This behavior is similar in the Bi-2212 compound [6-9]. The important contribution to the DOS above E_F comes mainly from the Bi p states with a contribution of the O3 p and O4 p states. These oxygen states have a major contribution below E_F . The DOS has a minor contribution from both Sr and Ca atoms due to their strong ionic character (not shown in the Fig. 2).

We also calculated the total spin magnetic moment per cell for Bi-2223 compound and obtained $0.011 \mu_B$, whose

main contribution is due to the Cu atoms. This implies that the compound does not exhibit a significant magnetic character at $T = 0$ K.

4.2. The band structure

The band structure of the Bi-2223 compound is shown in Fig. 3 (notice that \bar{M} is the midpoint between the Γ and Z points along the Σ direction).

This band structure has many features in common with the Bi-2212 compound [6-9]. In the band structure, the states just below E_F are primarily Cu2(3d), O2(2p), Cu1(3d) and O1(2p) states, with a small contribution from Bi(6p), O4(2p) and O3(2p) states. Above E_F , most of the states are Bi(6p), O4(2p) and O3(2p) with a minor contribution from states from the Cu-O planes. As it can be seen in the Fig. 3(A), the band dispersion in the Γ -Z direction (perpendicular to the basal plane) is minimal which means that the bands are strongly two dimensional.

There are five bands crossing at E_F which are composed primarily of Cu2 $d_{x^2-y^2}$ and O2 $p_{x,y}$ (in red), Cu1 $d_{x^2-y^2}$ and O1 $p_{x,y}$ (in green), Bi $p_{x,y}$, O4 $p_{x,y}$ and O3 $p_{x,y}$ (in blue) states in Fig. 3 (Color online). The hybridized states from these bands are represented by their respective color mixture and the black line represents the other states. In Table III we present in detail the contribution at E_F from the different atomic states.

These bands cross E_F in two regions, the first one between the Z-X points and the second one near the \bar{M} point. In the first region (inset inside Fig. 3(A)) there are three nearly

TABLE III. Detailed contribution from the different atomic states to the bands at E_F .

Direction	Band	Bi	O4	O3	Cu1	O1	Cu2		O2
		$p_{x,y}$	$p_{x,y}$	$p_{x,y,z}$	$d_{x^2-y^2}$	$p_{x,y}$	$d_{x^2-y^2}$	d_{z^2}	$p_{x,y}$
Z-X	α	-	-	-	29%	25%	29%	-	17%
	β	-	-	-	-	-	62%	-	38%
	γ	-	-	-	28%	24%	29%	-	19%
Γ -Z (Σ)	δ	44%	24%	25%	-	-	4%	-	3%
Γ - \bar{M}	ε	33%	9%	19%	6%	3%	16%	6%	8%
\bar{M} -Z	ε	47%	13%	27%	-	-	6%	-	11%
\bar{M} -X	α	-	-	-	44%	16%	29%	-	11%
	β	18%	12%	8%	-	-	45%	-	17%
	γ	42%	25%	19%	10%	4%	-	-	-
	δ	17%	7%	11%	-	-	47%	-	18%
	ε	-	-	-	24%	8%	46%	7%	15%

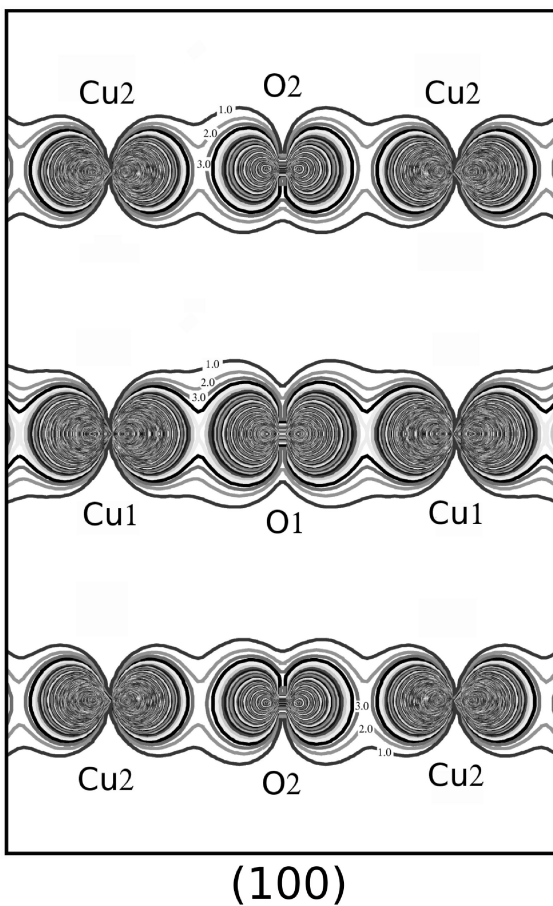


FIGURE 4. Charge density contour plots for the α band at E_F in the Z-X direction, on the (100) plane cutting the Cu1-O1 and Cu2-O2 bonds. Contours are given on a linear scale which values are $10^{-3}e/a.u^3$.

degenerate bands, two of them labeled as α and γ , are composed of Cu1 d , O1 p , Cu2 d , and O2 p states (see Table III).

In order to show the character of the α band at E_F , we plot in Fig. 4 the corresponding contour plots of the charge density, calculated at $k = 2\pi(0.19/a, 0.19/b, 0.61/c)$ on the (100) plane cutting the Cu1-O1 and Cu2-O2 bonds. There we see that the Cu-O states are bonding very similar to the corresponding Cu-O states of the Bi-2212 compound [8]. The other band (labeled as β) is also composed of bonding Cu2 d and O2 p states. These three bands (see inset inside Fig. 3(A)) give the higher contribution to the DOS at the Fermi level.

In the second region (near the \bar{M} point), the behavior of the bands are different along the Γ -Z (in Σ direction) and the \bar{M} -X directions (see shaded areas in Fig. 3(A)). Further, as seen in Fig. 3(B) there are two bands, labeled as δ and ε , crossing at E_F in the Σ direction, which are non symmetric around the \bar{M} point. Between the Γ and Z points, the δ band is composed of weakly bonding Bi p -O4 p and anti-bonding Bi p -O3 p states. The ε band between the Γ and \bar{M} points, is formed of anti-bonding Bi p -O4 p and Bi p -O3 p states and hybridizes with Cu2 d -O2 p and Cu1 d -O1 p states, with a small contribution from Cu2 d_{z^2} states, while between the \bar{M} and Z points it is composed of anti-bonding Bi p -O4 p states and hybridizes with Cu2 d -O2 p and O3 p states. In Fig. 5 we show the contour plots of the charge density in the (100) and (110) planes, cutting the Bi-O and Cu-O bonds corresponding to the ε band in Fig. 3(B) at $k = 2\pi(0.42/a, 0, 0)$, very close to E_F . Figure 5(A) shows the strong Bi-Bi bonding character ($pp\sigma$) and the anti-bonding character of the Cu-O planes. In Fig. 5(B) we show the contour plot of the charge density on the (110) plane. There we can see the anti-bonding character of the Bi-O and Cu2-O3 states. This behavior is similar to the one reported for Bi-2212 by Massidda *et al.* [5].

Around the \bar{M} point but in the \bar{M} -X direction (see Fig. 3(C)), the α , β , γ , δ and ε bands have a different character. The α band is a combination of bonding Cu1 d -O1 p and Cu2 d -O2 p states (see Table III). The β and δ bands are

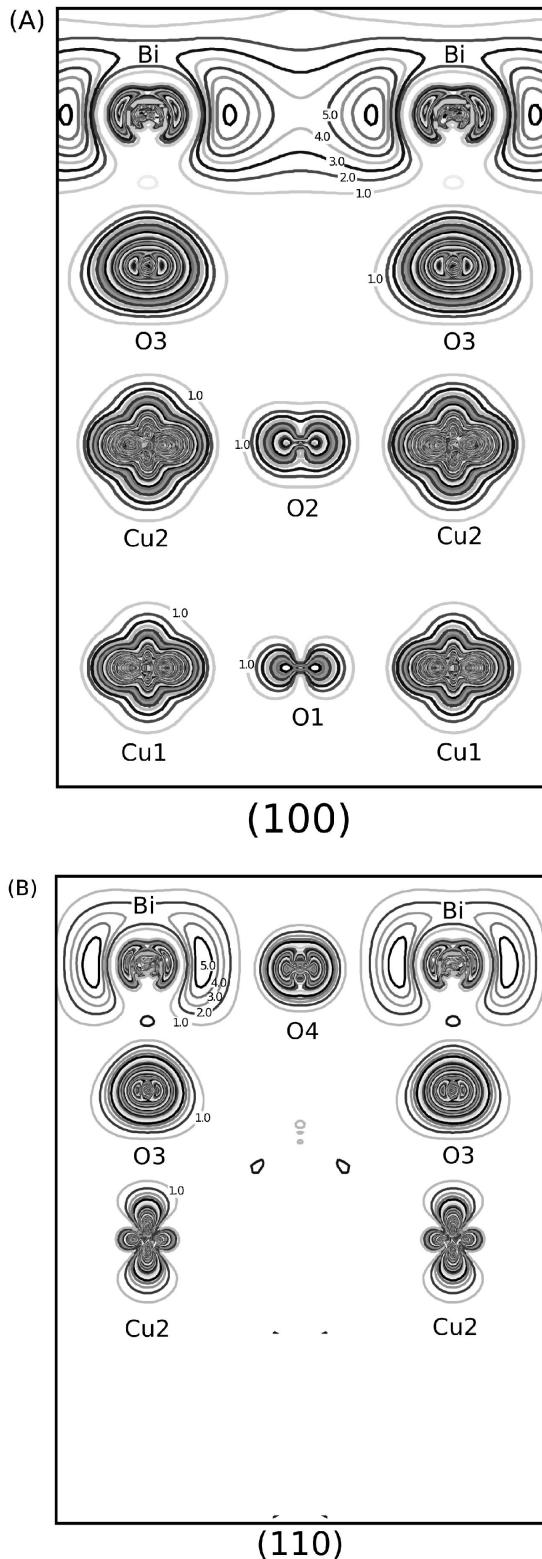


FIGURE 5. Charge density contour plots for the ϵ band at E_F in Γ - \bar{M} direction, in the (100) and (110) planes. Note the bonding character of Bi-Bi bonds and the anti-bonding character of Cu-O bonds in (100) plane. In (110) plane the contribution of the Cu1-O1 plane is not observed (see text). Contours are given as in Fig. 4.

composed of hybrids of bonding Cu2 d -O2 p , anti-bonding Bi p -O4 p and Bi p -O3 p states. The γ band is composed of weakly bonding Bi p -O4 and Bi p -O3 p states, and hybridizes with anti-bonding Cu1 d -O1 p states. Finally, the ϵ band has a similar behavior as the α band but with a small contributions of the Cu2 d_{z^2} state at E_F (see Table III).

In the Fig. 3(A), the copper-oxygen bands that cross at E_F extend from 1.5 eV below to 2.3 eV above E_F . These bands have their maximum energy at the X point, and their minimal energy at the Z point and are anti-bonding. These bands present a strong Cu-O $dp\sigma$ character. Around the \bar{M} point, the Bi-O bands extend to about 0.57 eV below E_F and hybridize with Cu2 $d_{x^2-y^2}$ -O2 p_y states. The Bi-O bands presents a $pp\sigma$ character. The contribution of the Bi-O states at E_F are due to the interaction with the O3 and the Cu2-O2 planes. The Bismuth bands present an interesting feature around Γ and Z. Exactly at those points, the band derives from only p_z state, while around those points the band derives from combinations of all p states.

The bands around the X point are ~ 0.54 eV below E_F while in the Bi-2212 compound this bands lie about ~ 0.1 eV below E_F [6-9]. These bands are primarily antibonding Cu1 $d_{xz,yz}$ -O1 p_z and Cu2 $d_{xz,yz}$ -O2 p_z states with a $dp\pi$ character. Taking the band structures of $\text{Bi}_2\text{Sr}_2\text{Ca}_{n-1}\text{Cu}_n\text{O}_y$ compounds with $n = 1$ and 2, calculated by Sterne and Wang [10] and comparing with our calculation ($n = 3$), we observed that the number of bands crossing at E_F in Γ -X direction is proportional to the number of Cu-O planes. A similar idea has been outlined by Mori *et al.* [33]. We also noted that the energy below E_F of the Bi-O bands around \bar{M} point is deeper proportionally to the number of Cu-O planes.

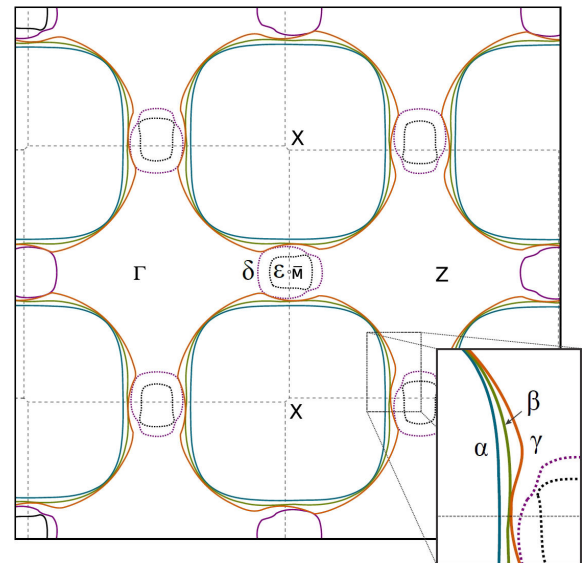


FIGURE 6. (Color online) The Fermi Surface at $k_z = 0$ of $\text{Bi}_2\text{Sr}_2\text{Ca}_2\text{Cu}_3\text{O}_{10}$ in an extended zone scheme. The Bi-O pockets are represented by violet and black lines (dashed lines).

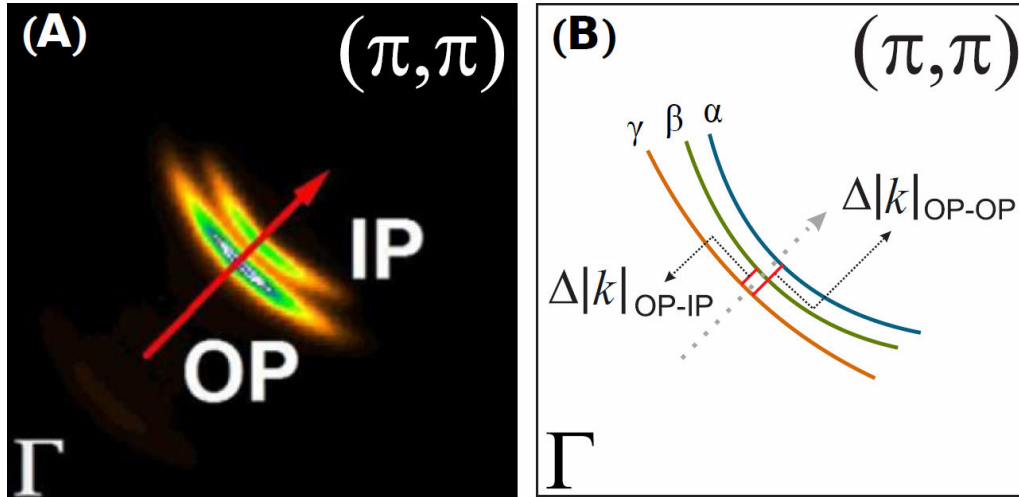


FIGURE 7. (Color online) (A) The Fermi surface (FS) of Bi-2223 measured by Ideta *et al.* using ARPES [23] in the nodal direction. (B) Schematic FS showing the band splitting and the $\Delta|k|$ calculated in this work. Experimental FS is taken from the Ref. [23].

4.3. The Fermi surface

In Fig. 6 we show the Fermi Surface (FS) of the Bi-2223 compound in an extended zone scheme. This FS has in general the same behavior to the one reported for the Bi-2212 compound, with the similar highly anisotropic low-dimensionality [8,9,34]. Our calculation presents two additional surfaces. Around the X there are three not quite degenerate hole surfaces labeled as α , β and γ (corresponding to the respective bands in Fig. 3). In Γ -X and equivalent directions, the α and γ surfaces consists of hybrids of Cu1-O1 and Cu2-O2 states and the β surface is composed of Cu2-O2 states. The α and the β surfaces are close to be rounded squares. As we approach from the X to the \bar{M} point, the β and the γ surfaces get an additional contribution from Bi-O4 states (see Table III). As we can see from Fig. 6 the α surface has more nesting than β and γ surfaces.

The FS of Bi-2223 measured by ARPES is shown in Ref. 23. In that work they found two surfaces on the nodal direction (see Fig. 7), that they call outer copper planes (OP) and inner copper plane (IP) and suggest the possibility that OP's are degenerate. The full width at half maximum (FWHM) of the momentum distribution curve (ARPES resolution) for the OP is $\sim 0.011 \text{ \AA}^{-1}$ and the IP is $\sim 0.0074 \text{ \AA}^{-1}$, at E_F . Other experimental works using the same technique [21,22] do not report this band splitting.

We identified the IP with the α surface and the OP's with the β and γ surfaces in our FS. On the Γ -X direction we calculated the differences in momentum $\Delta|k|_{OP-IP}$ and $\Delta|k|_{OP-OP}$ (see Fig. 7) and found $\sim 0.005 \text{ \AA}^{-1}$ and $\sim 0.01 \text{ \AA}^{-1}$ respectively. Comparing these differences with the ARPES resolution in the work just mentioned, it is clear that it cannot resolve the existence of the three bands separately. Our results support the idea that the IP is composed of Cu2-O2 states, and the OP's are composed of hybrids of Cu1-O1 and Cu2-O2 states.

Now, around the \bar{M} point we observe two surfaces (Bi-O pockets) in comparison with the single surface observed in the Bi-2212 compound. These surfaces, labeled as δ and ε (see Fig. 6) form small closed electron surfaces. The δ surface is close to be a rounded square with a small convexity pointing towards the Z point, while ε surface is almost a rounded rectangle. In the experimental reports the Bi-O planes show always a nonmetallic character [31]. In the theoretical calculations this is called the ‘‘Bi-O pockets problem’’, meaning the presence of Bi-O bands at E_F around the high symmetry point \bar{M} in the irreducible Brillouin zone (IBZ). This problem appears in all the bismuth cuprates, a result which does not correspond to the experiment [35].

We associate the Bi-O pockets problem as coming from the interaction of the Cu2-O2 and Bi-O4 planes through O3 atoms (the ones associated to the Sr-O planes). The ionic character of the Bi atoms in the crystalline structure tend to attract electrons into the Bi-O planes competing with the affinity for the electrons towards the Cu-O planes [35]. This may involve the charge transfer between the Cu2-O2 and Bi-O4 planes. This charge transfer is possible by the interaction of the O3 atoms with the aforementioned planes, giving these Bi-O4 planes the metallic character observed in our calculation. We believe that is possible to remove the Bi-O pockets by displacing the O3 atoms in order to avoid the interaction between the Cu2-O2 and Bi-O4 planes.

Finally, around the Γ and Z points there are electron surfaces that are similar between them. This characteristic is due to the highly two-dimensionality of the system. However from the band structure and the FS of the Bi-2223 compound we observe a less two dimensional behavior than the one reported for the Bi-2212 compound [8,9].

5. Conclusions

We presented in this paper a detailed analysis of the electronic properties of the tetragonal ($I4/mmm$) Bi-2223 com-

pound. Our calculation was done using the Full-potential linearized augmented plane wave method plus Local orbitals within the Local density approximation using Wien2k code.

We studied the contribution of the Cu1-O1 plane to the electronic properties of the Bi-2223 compound. This plane has an important contribution to the DOS at the E_F (0.56 states/eV-atom) which is similar to the one of the Cu2-O2 plane. Compared to Bi-2212 [9], Bi-2223 presents a higher DOS at E_F . This is due to the new Cu-O plane.

Our calculated band structure present Bi-O bands at the E_F . This so called Bi-O pocket problem is in disagreement with the experimental results. This problem also appears in the theoretical calculations concerning Bi-2212 and Bi-2201. Taking the band structures of Bi-2212 and Bi-2201 [10] and comparing with our calculation (Bi-2223), we observed that the number of bands crossing at E_F in Γ -X direction is proportional to the number of Cu-O planes. This is in agreement with the idea outlined by Mori *et al.* [33]. We also noted that the energy below E_F of the Bi-O bands around \bar{M} point is deeper proportionally to the number of Cu-O planes.

The Fermi surface (FS) calculated in this work presents a good agreement with the experimental result measured, in the nodal direction, by angle-resolved photo-emission spectroscopy (ARPES) [23].

Acknowledgments

The authors acknowledge to the GENERAL COORDINATION OF INFORMATION AND COMMUNICATIONS TECHNOLOGIES (CGSTIC) at CINVESTAV for providing HPC resources on the Hybrid Cluster Supercomputer Xiuhcoatl and to the Instituto de Ciencia y Tecnología del Distrito Federal under the contract ICyTDF/268/2011, that have contributed to the research results reported within this paper. J.A.C.M. acknowledges the support of Conacyt México through a PhD scholarship. D.E. acknowledges the hospitality of the Department of Physics at Cinvestav.

1. S. A. Sunshine *et al.*, *Phys. Rev. B* **38** (1988) 893.
2. A. Maeda, M. Hase, I. Tsukada, K. Noda, S. Takebayashi, and K. Uchinokura, *Phys. Rev. B* **41** (1990) 6418.
3. J. L. Tallon *et al.*, *Nature* **333** (1988) 153.
4. J. M. Tarascon *et al.*, *Phys. Rev. B* **38** (1988) 8885.
5. P.V. Bogdanov *et al.*, *Phys. Rev. B* **64** (2001) 180505. An references there in.
6. M. S. Hybertsen and L. F. Mattheiss, *Phys. Rev. Lett.* **60** (1988) 1661.
7. L. F. Mattheiss and D. R. Hamann, *Phys. Rev. B* **38** (1988) 5012.
8. S. Massidda, J. Yu and A. J. Freeman, *Phys. C* **152** (1988) 251.
9. H. Krakauer and W. E. Pickett, *Phys. Rev. Lett.* **60** (1988) 1665.
10. P. A. Sterne and C. S. Wang, *J. Phys. C: Solid State Phys.* **21** (1988) L949.
11. Kitaguchi H and Kumakura H. *MRS Bulletin: Advances in Bi-Based High-Tc Superconducting Tapes and Wires* **26** (2001) 121.
12. T. J. Arndt, A. Aubele, H. Krauth, M. Munz, B. Sailer, and A. Szulczyk, *IEEE Transactions on Applied Superconductivity* **13** (2003) 3030.
13. W. Hassenzahl, *et al. Electric power applications of superconductivity. Proceedings of the IEEE. Special Issue on Applications of Superconductivity* **92** (2004) 1655.
14. V. F. Shamray, A. B. Mikhailova, and A. V. Mitin, *Crystallography Reports* **54** (2009) 584.
15. A. Sequeira A, J.V. Yakhmi, R.M. Iyer, H. Rajagopal and P.V.P.S.S. Sastry, *Physica C* **167** (1990) 291.
16. W. Carrillo-Cabrera and W. Gopel, *Phys. C* **161** (1989) 373.
17. X. Zhu, S. Feng, J. Zhang, G. Lu, K. Chen, K. Wu, Z. Gan, *Modern Phys. Lett. B* **3** (1989) 707.
18. J. Yang, C. Ye, B. Zhang, J. Li, J. Kang, Y. Ding, Y. He, J. Zhang, A. He, J. Xiang, *Modern Physics Letters B* **4** (1990) 791.
19. G. Miede, T. Vogt, H. Fuess and M. Wilhelm, *Phys. C* **171** (1990) 339.
20. E. Giannini, R. Gladyshevskii, N. Clayton, N. Musolino, V. Garnier, A. Piriou, R. Flukiger, *Current Applied Physics* **8** (2008) 115.
21. D. L. Feng *et al.*, *Phys. Rev. Lett.* **88** (2002) 107001.
22. H. Matsui *et al.*, *Phys. Rev. B* **67** (2003) 060501.
23. S. Ideta *et al.*, *Phys. Rev. Lett.* **104** (2010) 227001.
24. S. Ideta *et al.*, *Phys. C* **470** (2010) S14.
25. O. K. Andersen, *Phys.Rev.B* **12** (1975) 3060.
26. P. Blaha, K. Schwars, G.K.H. Madsen, D. Kvasnicka, and J. Luitz, *WIEN2K: Full Potential-Linearized Augmented Plane waves and Local Orbital Programs for Calculating Crystal Properties*, edited by K. Schwars, (Vienna University of Technology, Austria, 2001).
27. L. F. Mattheiss, *Phys. Rev. Lett.* **58** (1987) 1028.
28. L. F. Mattheiss and D. R. Hamann, *Solid State Commun.* **63** (1987) 395.
29. S. Massidda, J. Yu, A. J. Freeman, and D. D. Koelling, *Phys. Lett. A* **122** (1987) 198.
30. D. R. Hamann and L. F. Mattheiss, *Phys. Rev. B* **38** (1988) 5138.
31. M. Tanaka *et al.*, *Nature* **339** (1989) 691.
32. A. Damascelli *et al.*, *Rev. Mod. Phys.* **75** (2003) 473.
33. M. Mori, T. Tohyama, and S. Maekawa, *Phys. Rev. B* **66** (2002) 064502.
34. V. Bellini, F. Manghi, T. Thonhauser and C. Ambrosch-Draxl, *Phys.Rev.B* **69** (2004) 184508.
35. Hsin Lin *et al.*, *Phys. Rev. Lett.* **96** (2006) 097001.